


Dark matter constraints from the eccentric supermassive black hole binary OJ 287

Ahmad Alachkar¹, John Ellis^{1,2,3} and Malcolm Fairbairn¹

¹King's College London, Strand, London, WC2R 2LS, United Kingdom

²Theoretical Physics Department, CERN, Geneva, Switzerland

³National Institute of Chemical Physics and Biophysics, R vala 10, 10143 Tallinn, Estonia

 (Received 29 July 2022; revised 13 January 2023; accepted 30 March 2023; published 18 May 2023)

OJ 287 is a blazar thought to be a binary system containing a $\simeq 18$ billion solar mass primary black hole accompanied by a $\simeq 150$ million solar mass secondary black hole in an eccentric orbit, which triggers electromagnetic flares twice in every $\simeq 12$ year orbital period when it traverses the accretion disk of the primary. The times of these emissions are consistent with the predictions of general relativity calculated to the 4.5th post-Newtonian order. The orbit of the secondary black hole samples the gravitational field at distances between $\mathcal{O}(10)$ and $\mathcal{O}(50)$ Schwarzschild radii around the primary, and hence is sensitive to the possible presence of a dark matter spike around it. We find that the agreement of general-relativistic calculations with the measured timings of flares from OJ 287 constrains the mass of such a spike to $\lesssim 3\%$ of the primary mass.

DOI: [10.1103/PhysRevD.107.103033](https://doi.org/10.1103/PhysRevD.107.103033)

OJ 287 is an active galactic nucleus (AGN) situated near the ecliptic in the constellation of Cancer at a cosmological redshift $z = 0.3056$ [1,2]. It is categorized as a BL Lacertae (BL Lac) object with a relativistic jet aligned very close to our line of sight [3]. Due to its proximity to the ecliptic, OJ 287 was often unintentionally photographed in the past, with an optical database dating back to 1888 [4–8], in addition to dedicated observing programs [8–10]. This huge dataset contains quasiperiodic pairs of electromagnetic flares every ~ 12 years [11], which are explained by Lehto and Valtonen [12,13] as impacts of a secondary black hole (BH) with the accretion disk of the primary BH as it describes an eccentric orbit. These impacts occur during periapsis approach and retreat, and the intervals between the flares are modulated by the precession of the orbit and the emission of gravitational waves [14–16].

In this scenario, the secondary BH punches through the geometrically thin, optically thick and radiation-dominated accretion disk of the primary BH with hypersonic velocity, shocking gas and generating hot bubbles of plasma on each side of the disk that expand, cool down adiabatically and eventually radiate by thermal bremsstrahlung after becoming optically thin [12,13], producing the observed flares [17]. The time delay between the emergence of a bubble at

the impact site and the epoch when it becomes transparent is an important aspect of the binary BH model. While this can be estimated via detailed astrophysical modeling of the disk impact shock and outflow evolution [18], it necessarily introduces some uncertainty into the calculations.

The observations constrain the primary BH to have a mass $\sim 18.35 \times 10^9 M_\odot$ [15], with the secondary BH having a mass $\sim 150 \times 10^6 M_\odot$. The orbit of the secondary BH has an eccentricity of ~ 0.65 , with a periapsis ~ 9 and an apoapsis ~ 48 times the primary's Schwarzschild radius, which is ~ 360 AU. These properties make OJ 287 a very powerful laboratory for probing general relativity (GR) and other aspects of fundamental physics. The GR predictions for the binary system have been calculated to 4.5th post-Newtonian order, including the dissipative effects of the emission of gravitational waves, and these calculations have been used to predict successfully the time of the 2019 burst of electromagnetic emission, which arrived within a few hours of the predicted time [15].

In this paper we use the successful comparison of GR predictions with the data on this unique astrophysical system to provide for the first time a constraint on physics beyond the Standard Model of particle physics, specifically on models of dark matter. It was argued in [19] that if cold dark matter is present at the center of a galaxy, a massive central BH distributes it adiabatically into a “spike” with a radial profile of the form

$$\rho(r) \propto F(r) \left(\frac{R_{\text{sp}}}{r} \right)^{\gamma_{\text{sp}}}, \quad (1)$$

Published by the American Physical Society under the terms of the [Creative Commons Attribution 4.0 International license](https://creativecommons.org/licenses/by/4.0/). Further distribution of this work must maintain attribution to the author(s) and the published article's title, journal citation, and DOI.

with $F(r) = (1 - 2R_S/r)^3$, where R_S is the Schwarzschild radius of the BH, and R_{sp} scales the size of the spike. (See [20,21] for a critique of the possible existence of a spike.) The density slope parameter, γ_{sp} , is expected to lie between 2.25 and 2.5. The total mass of cold dark matter in the spike is obtained by integrating (1) over r until the density sinks below the normal galactic dark matter density, and is unknown *a priori* because of the unknown normalization of $F(r)$ that depends on the BH being considered and its environment.

Evidence for the existence of such a spike has been sought in the center of the Milky Way. In particular, measurements of the orbit of the star S2, whose orbit samples the gravitational field of Sgr A* down to radii $\sim 10^{-2}$ pc, were found in [22] to constrain the spike mass to $\sim 1\%$ of the mass of Sgr A*, assuming $\gamma_{sp} = 7/3$ and $R_{sp} = 100$ pc, the upper limit obtained from VLT measurements of the orbit of S2. (A weaker constraint is provided by the concordance between the estimates of the mass of Sgr A* based on these orbital measurements and the radius of the innermost stable circular orbit measured by the Event Horizon Telescope, $r_{ISCO} \simeq 50 \mu\text{as}$ [23], which requires that the spike mass be $\lesssim 10\%$ of the mass of Sgr A*.)

The eccentricity of the orbit of the secondary BH in the OJ 287 system implies that it is sensitive to the density of any such spike around the primary BH at radii between the binary separations at periastris and apoapsis, potentially causing deviations from the GR predictions. We use simulations to model these deviations and fit the OJ 287 data with modified parameters that include dark matter spikes of different magnitudes. We treat the gravitational effects of the spike in the Newtonian approximation, assuming that it is centred on the primary black hole and spherical, that shells with radii less than the separation between the primary and secondary have the same effect as a pointlike mass co-located with the primary, and that the effects of shells with radii larger than the separation can be neglected. We follow [22] in assuming $\gamma_{sp} = 7/3$, while we fix R_{sp} at $5R_S$ (of the primary BH) throughout the analysis, and allow ρ_{sp} to vary such that the total DM mass enclosed within a region $2R_S \lesssim r \lesssim 50R_S$ (encompassing the trajectory traversed by the secondary BH around the primary from periastris to apoapsis) equals the studied m_{sp}/m_1 ratio (ranging from 0 to 0.03). This is well within the gravitational radius of influence of the primary BH (defined as the radius at which the enclosed DM mass is twice the mass of the primary BH). We neglect dynamical friction and post-Newtonian effects due to the spike, which is justified *a posteriori* by the upper limit on its mass that we establish.

We use the post-Newtonian (PN) scheme to calculate the orbital dynamics up to 4.5PN order. We work in the centre-of-mass (CoM) frame, converting the two-body problem to an effective one-body problem, and use harmonic coordinates. The harmonic condition, (de Donder gauge) is imposed, breaking general covariance. The relative two-body

acceleration and the precessional dynamics of the spin of the primary, written in terms of the unit vector \mathbf{s}_1 , can be estimated using

$$\begin{aligned} \ddot{\mathbf{x}} \equiv \frac{d^2\mathbf{x}}{dt^2} &= \ddot{\mathbf{x}}_0 + \ddot{\mathbf{x}}_{1\text{PN}} + \ddot{\mathbf{x}}_{2\text{PN}} + \ddot{\mathbf{x}}_{3\text{PN}} \\ &+ \ddot{\mathbf{x}}_{2.5\text{PN}} + \ddot{\mathbf{x}}_{3.5\text{PN}} + \ddot{\mathbf{x}}_{4\text{PN}(\text{tail})} + \ddot{\mathbf{x}}_{4.5\text{PN}} \\ &+ \ddot{\mathbf{x}}_{\text{SO}} + \ddot{\mathbf{x}}_{\text{SS}} + \ddot{\mathbf{x}}_{\text{Q}} + \ddot{\mathbf{x}}_{4\text{PN}(\text{SO-RR})} \\ \frac{d\mathbf{s}_1}{dt} &= (\boldsymbol{\Omega}_{\text{SO}} + \boldsymbol{\Omega}_{\text{SS}} + \boldsymbol{\Omega}_{\text{Q}}) \times \mathbf{s}_1, \end{aligned} \quad (2)$$

where $\mathbf{x} = \mathbf{x}_1 - \mathbf{x}_2$ is the CoM relative separation vector between the BHs with masses m_1 and m_2 , $\ddot{\mathbf{x}}_0 = -\frac{Gm}{r^3}\mathbf{x}$ is the zeroth-order Newtonian acceleration, where m is the total mass of the binary and $r = |\mathbf{x}|$, and $\mathbf{S}_1 = \frac{Gm^2\chi_1}{c}\mathbf{s}_1$ is the spin of the primary with the Kerr parameter $\chi \in [0, 1]$ in GR. The terms $\ddot{\mathbf{x}}_{\text{SO}}$ and $\ddot{\mathbf{x}}_{\text{SS}}$ denote the spin-orbit (SO) and spin-spin (SS) couplings in GR, entering at 1.5PN and 2PN at leading orders, while $\ddot{\mathbf{x}}_{\text{Q}}$ is the classical spin-orbit coupling (Q) arising from the quadrupole deformation of a Kerr BH, at 2PN order, and the $\boldsymbol{\Omega}_i$ are the SO, SS and Q contributions to the precession of the primary BH spin vector. Our calculations of the various terms in (2) are based on an extensive body of work [24–29] and will be set out in detail in an upcoming publication.

The baseline binary BH model has 9 relevant parameters: the two BH masses $m_{1,2}$, the primary BH Kerr parameter χ_1 , the initial apocenter eccentricity e_0 , the initial semi-major axis a and its angle of orientation θ_0 , an ambiguity parameter γ for the leading-order hereditary contributions to GW emission in the BBH dynamics implemented following Eq. (5) in [15], an azimuthal angle θ_{S1} and a polar angle ψ_{S1} parametrizing the orientation of the primary spin vector.

When making fits, the plane-crossing epochs must be corrected to incorporate astrophysical processes between an impact and an observed optical outburst, with a time delay t_{del} added to account for the time lag between the generation of the plasma bubbles and the epoch at which they become optically thin. An additional timing correction t_{adv} is applied to model the tidal force of the approaching secondary BH that warps the disk and advances the impacts. We adopt empirical models of the time delay and advance based on the best-fit orbit of [15], which our good fits resemble. In our orbital fitting procedure, the observational uncertainties are all assumed to be Gaussian and uncorrelated, and the optimization algorithm adopted is the Nelder-Mead algorithm [30], which we implement using the `constrNMPy` package.

Figure 1 displays the evolution of the OJ 287 system in our best no-DM fit over a period of 120 y, corresponding to 10 orbits of the secondary BH (represented by the smaller black spot), in a coordinate system centred on the primary BH (represented by the larger black spot). We see clearly

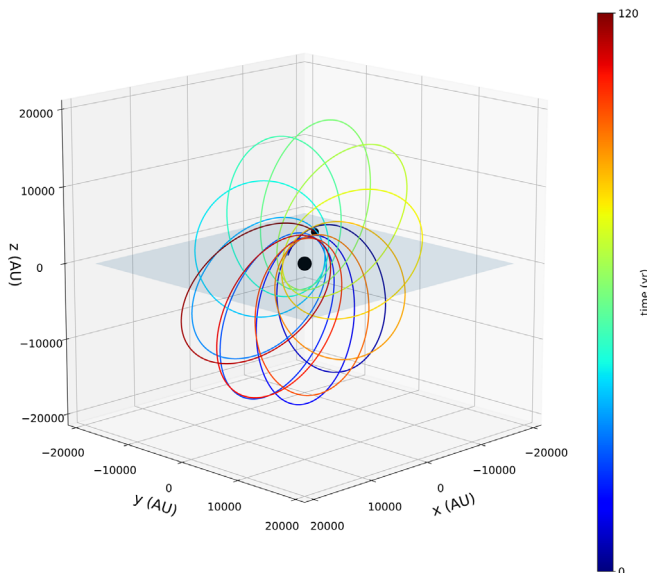


FIG. 1. The precessing orbit of the secondary BH (smaller black spot) in a coordinate system centered on the primary BH (larger black spot). Note the passages of the secondary BH through the accretion disc (represented as a shaded plane).

the large orbital precession and the passages of the secondary BH through the accretion disc (represented as a shaded plane) as it approaches and retreats from the periastron.

Table I lists in the first column the starting times of flares of OJ 287 starting with that at the end of 1912, with the corresponding uncertainties shown in the second column. The timings of the flares not written in bold were not measured accurately and are not used in our fits. Reference [15] used 10 flares, corresponding to 9 time differences that they fitted using the 9 parameters listed above. In our analysis we have one additional parameter characterizing the spike, and our fits include the well-measured 2019 flare as well as the less accurately measured flares in 1959 and 1994. The contribution of the spike to the dynamics is included at zeroth order and follows the mass profile obtained from (1). The third column in the Table lists the predictions for the starting times in our best-fit no-DM spike model, the fourth column is our best fit for a spike mass ratio $m_{\text{sp}}/m_1 = 0.02$, and the fifth column is that for a spike mass ratio of 0.03.

Figure 2 shows the minimum values of χ^2 that we found for the indicated choices of the spike mass ratio, m_{sp}/m_1 . The best-fit no-DM model has $\chi^2 = 6.05$, and the best fits for values of $m_{\text{sp}}/m_1 < 0.03$ all have $\chi^2 \lesssim 10$, corresponding to p -values $\gtrsim 20\%$. However, the best fit for $m_{\text{sp}}/m_1 = 0.03$ has $\chi^2 \simeq 13.6$, corresponding to a p -value $\simeq 3\%$, and the values of χ^2 rise sharply as m_{sp}/m_1 increases beyond 0.03. For example, $\chi^2 \simeq 99$ already for $m_{\text{sp}}/m_1 = 0.035$, corresponding to a p -value $\simeq 10^{-18}$. On the basis of these results we conclude that the current OJ 287 data set an upper limit $m_{\text{sp}}/m_1 \lesssim 0.03$.

TABLE I. Starting epochs (in Julian years) of the observed optical flares of OJ 287 from 1912 onwards. First column: The data points prior to 1970 were obtained from archival photographic plates while the historical 1912/3 flare time is from [8]. We only use the flares listed in bold, the starting times of the other flares are not known accurately and are not used in the fits. Second column: The uncertainties in the starting times. Third, fourth and fifth columns: Our predictions for the starting times in the best-fit no-DM spike model and in the best-fit models with spike mass ratios of 2% and 3%.

<i>Flare times, uncertainties and model estimates</i>				
Julian year	uncertainty	No spike	2% spike	3% spike
1912.980	± 0.020	1912.982	1912.968	1912.958
1922.529	...	1922.536	1922.537	1922.537
1923.725	...	1923.730	1923.725	1923.722
1934.335	...	1934.337	1934.340	1934.340
1935.398	...	1935.403	1935.402	1935.400
1945.818	...	1945.819	1945.822	1945.822
1947.283	± 0.002	1947.285	1947.284	1947.283
1957.095	± 0.025	1957.087	1957.078	1957.073
1959.25	± 0.05	1959.216	1959.213	1959.213
1964.231	...	1964.242	1964.216	1964.204
1971.126	...	1971.129	1971.127	1971.127
1972.935	± 0.012	1972.934	1972.921	1972.916
1982.964	± 0.0005	1982.964	1982.965	1982.965
1984.125	± 0.01	1984.120	1984.116	1984.114
1994.77	± 0.1	1994.595	1994.599	1994.599
1995.841	± 0.002	1995.839	1995.838	1995.838
2005.745	± 0.015	2005.747	2005.754	2005.754
2007.6915	± 0.0015	2007.693	2007.691	2007.692
2015.875	± 0.025	2015.882	2015.882	2015.872
2019.569	± 0.0005	2019.569	2019.568	2019.569

The upper panel of Fig. 3 compares the predictions of our best-fit models with no DM spike (shown as red spots), $m_{\text{sp}}/m_1 = 0.02$ (shown as blue crosses) and $m_{\text{sp}}/m_1 = 0.03$ (shown as purple triangles) with the observations

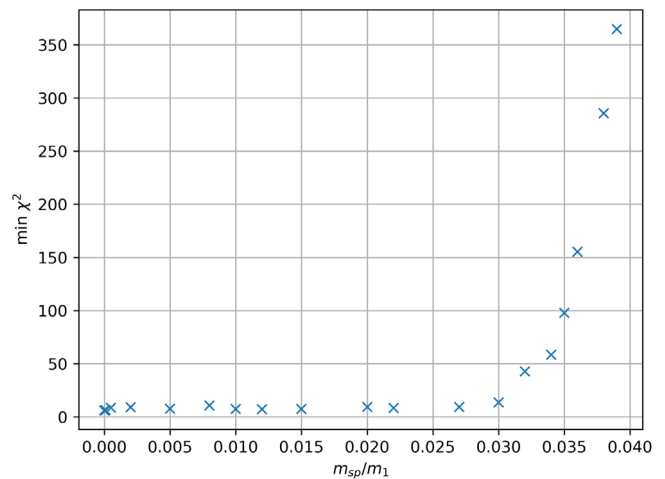


FIG. 2. The dependence of the χ^2 likelihood function on the ratio m_{sp}/m_1 , as obtained from the sampling of model parameters described in the text.

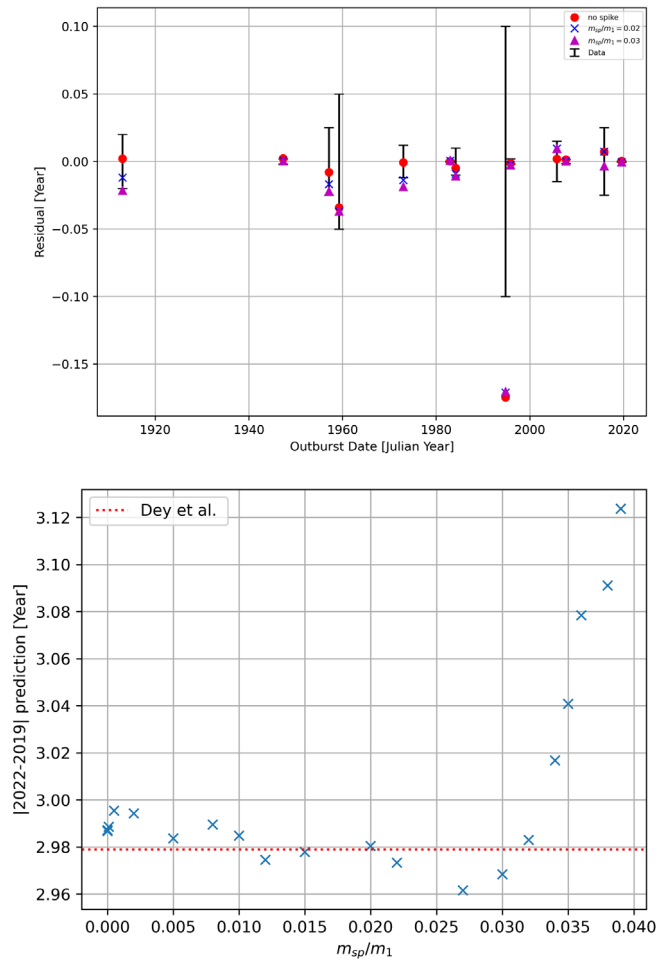


FIG. 3. Upper panel: the best-fit predictions for the flare timings calculated in a model without a dark matter spike (red spots), as obtained from the sampling of model parameters described in the text, compared with the measured timings (black). Also shown are the timings for the best fits with $m_{sp}/m_1 = 0.02$ (blue crosses) and $m_{sp}/m_1 = 0.03$ (purple triangles). Lower panel: a scatter plot of the predictions for the interval between the 2022 and 2019 flares (vertical axis) for our best fits with the indicated values of m_{sp}/m_1 (horizontal axis). We also show the prediction of [16] for the interval between the 2022 and 2019 flares (horizontal red dashed line).

(shown in black). We see a high level of consistency for the no-DM model, the most noticeable deviation being that for the 1994 flare. However, the observations of this flare were the least precise among the flares fitted, and its timing is the most uncertain, so we do not regard this deviation as being significant. There is also a good level of consistency for the best fit with $m_{sp}/m_1 = 0.02$. However, the best fit with $m_{sp}/m_1 = 0.03$ clearly does not fit the data as well, enabling the eye to confirm the numerical analysis presented in the previous paragraph.

Our no-DM spike prediction for the very well measured 2019 flare shown in Table I agrees with the measured timing to within a few hours, within the uncertainty in the

starting time of the 2019 flare. The timing of the 1982 flare is as well known as that in 2019, and our no-DM spike prediction for it again agrees with the measurement within a few hours.

As further support for our conclusion that $m_{sp}/m_1 \lesssim 0.03$, we have considered two possible side-effects of interactions between the secondary black hole and the spike. One is the dissipative effect of backreaction on the orbit of the secondary black hole, and the other is the possible disruption of the spike by the secondary black hole. Following the approach of [31], we find that both effects can be neglected in a first approximation.

According to the model of [14–16] another flare of OJ 287 is expected shortly, though there are considerable astrophysical uncertainties in its timing, as discussed in [16]. We now discuss how the timing of this flare might differ from the no-spike pure GR case discussed in [16]. As seen in the lower panel of Fig. 3, our estimates for $m_{sp}/m_1 \lesssim 0.03$ suggest that the next flare might be advanced by $\lesssim 5$ days relative to the no-spike prediction. On the other hand, we estimate that it would be delayed by > 10 days for $m_{sp}/m_1 \geq 0.035$. In view of the uncertainty in the arrival time estimated in [16], our results suggest that observations of the next flare of OJ 287 may not be able to strengthen our constraint $m_{sp}/m_1 \leq 0.03$ based on the timings of previous flares.

GR has already been tested by observations of OJ 287 to the 4.5PN order, including the effects of GW emission [16], and will be tested again by observations of future flares. We have shown in the paper, for the first time, how observations of OJ 287 can be used to constrain models of new physics beyond the Standard Model of particle physics. Specifically, observations of OJ 287 can constrain the possible existence of a cold dark matter spike surrounding its primary BH. They already constrain the possible mass of such a spike to $m_{sp}/m_1 < 0.03$ at the 99.9% C.L., and measurements of the timing of the expected future flares and more detailed modelling have the potential to constrain further the spike mass.

There are certainly ways in which the modeling of dark matter effects on the evolution of OJ 287 could be improved. For example, we have considered the possible static gravitational effects of a cold dark matter spike but have not considered other possible interactions between the secondary black hole and the spike, such as tidal forces or nongravitational interactions. Another important area for future research will be to refine the modeling of the dynamical interactions between the secondary black hole and the accretion disk, and the time delay between the nominal impact on the accretion disk and electromagnetic emissions from the cooling of the plasma bubble that it generates, which is the dominant uncertainty in the prediction of the timing of any future flare.

OJ 287 has barely begun to demonstrate its potential for probing not just astrophysics and GR, but also other aspects of fundamental physics.

ACKNOWLEDGMENTS

We are grateful to Mauri Valtonen and Pauli Pihajoki for fruitful discussions and valuable comments. The work of A. A. was supported by a UK STFC studentship, that of

J. E. and M. F. was supported in part by STFC Grants No. ST/P000258/1 and No. ST/T000759/1, and that of J. E. also in part by the Estonian Research Council via a Mobilitas Pluss grant.

-
- [1] M. L. Sitko and V. T. Junkkarinen, Continuum and line fluxes of OJ 287 at minimum light, *Publ. Astron. Soc. Pac.* **97**, 1158 (1985).
- [2] K. Nilsson, L. O. Takalo, H. J. Lehto, and A. Sillanpää, H-alpha monitoring of OJ 287 in 2005-08, *Astron. Astrophys.* **516**, A60 (2010).
- [3] W. A. Stein, S. L. O'Dell, and P. A. Strittmatter, The BL Lacertae objects, *Annu. Rev. Astron. Astrophys.* **14**, 173 (1976).
- [4] A. Sillanpää, S. Haarala, M. J. Valtonen, B. Sundelius, and G. G. Byrd, OJ 287: Binary pair of supermassive black holes, *Astrophys. J.* **325**, 628 (1988).
- [5] R. Hudec, L. Hudec, A. Sillanpää, L. Takalo, and P. Kröll, Long-term monitoring of OJ287: New data, In *Exploring the Gamma-Ray Universe*, A. Gimenez, V. Reglero, and C. Winkler, ESA Special Publication Vol. 459 (ESA Publications Division, Noordwijk, 2001), pp. 295–296.
- [6] N. Visvanathan and J. L. Elliot, Variations of the radio source OJ 287 at optical wavelengths, *Astrophys. J.* **179**, 721 (1973).
- [7] A. A. Abdo *et al.*, The spectral energy distribution of Fermi bright blazars, *Astrophys. J.* **716**, 30 (2010).
- [8] R. Hudec, M. Bašta, P. Pihajoki, and M. Valtonen, The historical 1900 and 1913 outbursts of the binary blazar candidate OJ 287, *Astron. Astrophys.* **559**, A20 (2013).
- [9] L. O. Takalo, Blazar continuum variability Astronomical Society of the Pacific Conference Series 110, in *Proceedings of an international workshop held at Florida International University, Miami, Florida, USA* (Astronomical Society Pacific, San Francisco, 1996), Vol. 110, p. 70.
- [10] Arti Goyal *et al.*, Stochastic modeling of multiwavelength variability of the classical BL Lac object OJ 287 on timescales ranging from decades to hours, *Astrophys. J.* **863**, 175 (2018).
- [11] M. J. Valtonen, H. J. Lehto, A. Sillanpää, K. Nilsson, S. Mikkola, R. Hudec, M. Basta, H. Teräsranta, S. Haque, and H. Rampadarath, Predicting the next outbursts of OJ 287 in 2006-2010, *Astrophys. J.* **646**, 36 (2006).
- [12] Harry J. Lehto and Mauri J. Valtonen, OJ 287 outburst structure and a binary black hole model, *Astrophys. J.* **460**, 207 (1996).
- [13] B. Sundelius, M. Wahde, H. J. Lehto, and M. J. Valtonen, A numerical simulation of the brightness variations of OJ 287, *Astrophys. J.* **484**, 180 (1997).
- [14] Mauri J. Valtonen *et al.*, A massive binary black-hole system in OJ 287 and a test of general relativity, *Nature (London)* **452**, 851 (2008).
- [15] Lankeswar Dey, M. J. Valtonen, A. Gopakumar, S. Zola, R. Hudec, P. Pihajoki, S. Ciprini, K. Matsumoto, K. Sadakane, M. Kidger *et al.*, Authenticating the presence of a relativistic massive black hole binary in OJ 287 using its general relativity centenary flare: Improved orbital parameters, *Astrophys. J.* **866**, 11 (2018).
- [16] Seppo Laine, Lankeswar Dey, Mauri Valtonen, A. Gopakumar, Stanislaw Zola, S. Komossa, Mark Kidger, Pauli Pihajoki, José L. Gómez, Daniel Caton *et al.*, Spitzer observations of the predicted Eddington flare from Blazar OJ 287, *Astrophys. J. Lett.* **894**, L1 (2020).
- [17] Harry J. Lehto and Mauri J. Valtonen, OJ 287 outburst structure and a binary black hole model, *Astrophys. J.* **460**, 207 (1996).
- [18] Pauli Pihajoki, Black hole accretion disc impacts, *Mon. Not. R. Astron. Soc.* **457**, 1145 (2016).
- [19] Paolo Gondolo and Joseph Silk, Dark Matter Annihilation at the Galactic Center, *Phys. Rev. Lett.* **83**, 1719 (1999).
- [20] Piero Ullio, Hongsheng Zhao, and Marc Kamionkowski, Dark-matter spike at the Galactic Center?, *Phys. Rev. D* **64**, 043504 (2001).
- [21] David Merritt, Milos Milosavljević, Licia Verde, and Raul Jimenez, Dark Matter Spikes and Annihilation Radiation from the Galactic Center, *Phys. Rev. Lett.* **88**, 191301 (2002).
- [22] Thomas Lacroix, Dynamical constraints on a dark matter spike at the galactic centre from stellar orbits, *Astron. Astrophys.* **619**, A46 (2018).
- [23] Kazunori Akiyama *et al.*, First Sagittarius A* Event Horizon Telescope Results. I. The shadow of the supermassive black hole in the center of the milky way, *Astrophys. J. Lett.* **930**, L12 (2022).
- [24] Bala R. Iyer and Clifford M. Will, Post-Newtonian Gravitational Radiation Reaction for Two-Body Systems, *Phys. Rev. Lett.* **70**, 113 (1993).
- [25] Bala R. Iyer and Clifford M. Will, Post-Newtonian gravitational radiation reaction for two-body systems: Nonspinning bodies, *Phys. Rev. D* **52**, 6882 (1995).
- [26] Piotr Jaranowski and Gerhard Schäfer, Radiative 3.5 post-Newtonian ADM Hamiltonian for many-body point-mass systems, *Phys. Rev. D* **55**, 4712 (1997).
- [27] Christian Königsdörffer, Guillaume Faye, and Gerhard Schäfer, Binary black-hole dynamics at the third-and-a-half post-Newtonian order in the ADM formalism, *Phys. Rev. D* **68**, 044004 (2003).
- [28] Yousuke Itoh, Third-and-a-half order post-Newtonian equations of motion for relativistic compact binaries using the strong field point particle limit, *Phys. Rev. D* **80**, 124003 (2009).

- [29] A. Gopakumar, Bala R. Iyer, and Sai Iyer, Second post-Newtonian gravitational radiation reaction for two-body systems: Nonspinning bodies, *Phys. Rev. D* **55**, 6030 (1997).
- [30] John A. Nelder and Roger Mead, A simplex method for function minimization, *Comput. J* **7**, 308 (1965).
- [31] Bradley J. Kavanagh, David A. Nichols, Gianfranco Bertone, and Daniele Gaggero, Detecting dark matter around black holes with gravitational waves: Effects of dark-matter dynamics on the gravitational waveform, *Phys. Rev. D* **102**, 083006 (2020).